AIAA JOURNAL
Vol. 38, No. 10, October 2000

Integrated Micro/Macro Approach for Laminate Composite Analysis: Applications to Turbine Blades

Antonio F. Ávila*
Universidade Federal de Minas Gerais, 31270-901 Belo Horizonte, Minas Gerais, Brazil

An integrated micro/macro mechanical procedure for structural analysis of unidirectional metal matrix composites is proposed. The micromechanical analysis is performed with the composite cylinder assemblage model or the representative volume element approach. The macroscopic stress–strain relation is based on a modification of the vanishing fiber diameter theory and the concept of a "smeared" finite element. The fibers are considered to be linear elastic, and the matrix viscoplastic behavior is described by the Bodner and Partom model (Bodner, S. R., "Review of Unified Elastic–Viscoplastic Theory," *Unified Constitutive Equations for Plastic Deformation and Creep of Engineering Alloys*, edited by A. Miller, Elsevier Science, New York, 1987, pp. 77–106). The overall composite behavior is assumed to be elastic–viscoplastic. Two types of material systems are used: SCS-6/Ti-15-3 and SCS-6/Tiβ21-S. Both sets of material systems exhibit isotropic and/or kinematic hardening under specific conditions of temperature and loading. The proposed methodology is validated with experimental and analytical results available in the literature. After the validation process, this methodology is applied to a three-dimensional finite element model of a $[0/90]_{2s}$ SCS-6/Tiβ21-S turbine blade tip. Aerodynamic and centrifugal loading are considered to be acting at the same time. The turbine blade tip inelastic strain field is presented.

Introduction

METAL matrix composites (MMCs) are in demand for use in many structural components in hostile environments. Among the MMC advantages over traditional materials are high-strength and elastic moduli, impact resistance, and toughness. The aeronautical field is only one of the numerous applications in which MMC can be used. For many years micromechanical models have been proposed to analyze composite material behavior. A micromechanical model can be described by different approaches such as asymptotic homogenization, variational techniques, and the representative volume element (RVE). Each one has its particular characteristics.

Asymptotic homogenization techniques have been used to describe the elastic, viscoelastic, and inelastic behavior of reinforced composite materials by researchers as Meguid and Kalamkarov,[1] Yi et al.,[2] and Fish et al.[3] Despite the good results of asymptotic homogenization (Fish et al.[3] reported only a 3% error on stress calculations), the computational efforts required are high compared with those of other techniques, e.g., variational formulations.

Variational formulations have been applied to composite materials since the 1950s, when Eshelby[4] proposed a model to compute effective properties of composite materials with ellipsoidal inclusions. Since the early 1960s, efforts have been made by Hashin et al.[5,6] to develop bounds for different types of composite materials. Willis,[7,8] Ponte Castañeda and Willis,[9] and Christensen[10] are among many researchers who developed new micromechanical models by applying energy principles in the 1980s. The work of Willis and Ponte Castañeda is focused on composite inelastic behavior, whereas Christensen studied elastic behavior. Talbot and Willis,[11] Luciano and Sacco,[12] Hashin,[13] and Ponte Castañeda[14] are a few of those who developed explicit expressions for the effective moduli and new bounds for elastic and inelastic behavior of composite materials in the 1990s. In spite of the huge amount of work done in this area, all of those models are limited to certain types of fiber/matrix configurations. One possible alternative solution is the application of the so-called RVE.

The use of a RVE has been applied to obtain the composite effective elastic moduli, as in recent works by Aboudi,[15] Sun and Vaidya,[16] and Drugan and Willis.[17] All of these works unfortunately do not connect the micromechanical analysis to the macromechanical one. The micro/macro mechanical analysis was attempted by Chun and Daniel[18] for the thermoelastoplastic analysis of a unidirectional MMC with the application of the Mori–Tanaka average field theory[19] and the concept of secant properties of the matrix. Kodiyalam et al.[20] also developed an integrated micro/macro model in which the micromechanical analysis was used as a pointer to correlate the lamina experimental and calculated properties. Aboudi et al.[21] also provided a coupled micro/macro continuum model. Their idea was the explicit coupling between Aboudi's classical model[15] and the composite macrostructure. They developed such a theory for functionally graded materials with good results. Another integrated micro/macro mechanical analysis was performed by Tamma and Ávila[22] for the elastic–viscoplastic analysis of unidirectional MMC, using the composite cylinder assemblage (CCA) model,[23] and the RVE approach and introduced a variation of the vanishing fiber diameter (VFD) theory.[24]

This paper focuses on the stress analysis of MMC structures in which an integrated micro/macro mechanical approach is considered. A model is proposed to describe the material behavior of MMCs that is transversely isotropic. The fibers are considered to behave in an elastic manner, and the matrix viscoplastic behavior is described by the constitutive model developed by Bodner and Partom (see Ref. 25). The overall composite behavior is assumed to be elastic–viscoplastic. A variation of the VFD theory is introduced and associated with the smeared-element concept, creating a new macroscopic stress–strain relation.

Integrated Micro/Macro Model

The micromechanical analysis can be performed with the CCA or the RVE approach. As bounds for the elastic moduli of a transversely isotropic composite were derived by Hashin,[23] they are not derived here; instead the attention is focused on the RVE model. Such an approach is more flexible because it allows the researcher to isolate a periodical microstructure and apply simple boundary conditions, i.e., single traction and pure shear, and from energy-conservation laws it is possible to obtain the composite effective moduli. An asymptotic homogenization procedure could also be applied, but the number of calculations would be quite substantial. According to Sun and Vaidya,[16] the RVE approach, based on displacement boundary conditions, leads to effective moduli lower bounds because of the application of the energy-balance laws. Therefore, the choice of the RVE is due to two factors: First, it is a less expensive computational model and, second, it has the possibility of obtaining the composite's effective moduli lower bounds.

Received 12 August 1998; revision received 10 February 2000; accepted for publication 6 March 2000.

*Department of Mechanical Engineering, 6227 Antonio Carlos Avenue; aavila@dedalus.lcc.ufmg.br. Member AIAA.

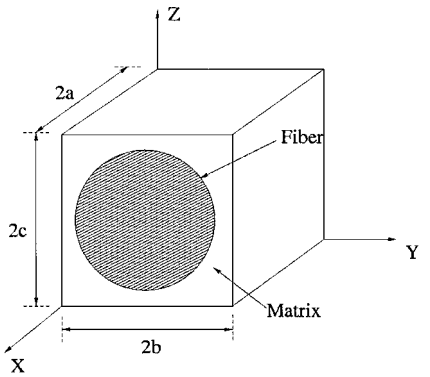

Fig. 1 RVE representation.

Assuming the usual Cartesian system, in which the x direction is the longitudinal axis, and considering the composite as an overall transversely isotropic material, a typical RVE can be represented by Fig. 1. A displacement ($u = u_0$) is imposed on $x = 2a$, and the other constrained displacements are set to zero. The normal constraint forces are calculated and denoted by F_x^1, F_y^1, and F_z^1, where the superscript indicates that these forces are from loading case 1. Next, a displacement ($v = v_0$) is imposed on $y = 2b$, and the other constrained displacements are set to zero. The corresponding constraint forces F_x^2, F_y^2, and F_z^2 are then calculated. Finally, a displacement ($w = w_0$) is imposed on $z = 2c$ and the other constrained displacements are set to zero. The constraint forces F_x^3, F_y^3, and F_z^3 are calculated next. These nine constraint forces are used in the following equations:

$$F_x^1 + \alpha F_x^2 + \beta F_x^3 = P \tag{1}$$

$$F_y^1 + \alpha F_y^2 + \beta F_y^3 = 0 \tag{2}$$

$$F_z^1 + \alpha F_z^2 + \beta F_z^3 = 0 \tag{3}$$

The unknowns are the load in the x direction, P, and the scaling coefficients α and β. Using algebraic manipulations, we can calculate the coefficients α and β Eqs. (2) and (3):

$$\alpha = \frac{-F_y^1 - \beta F_y^3}{F_y^2}, \qquad \beta = \frac{F_y^1 F_z^2 - F_y^2 F_z^1}{F_z^3 F_y^2 - F_y^3 F_z^2} \tag{4}$$

The average normal strains and the average Poisson ratio are defined as

$$\varepsilon = \left[\frac{u_0}{2a}, \frac{\alpha v_0}{2b}, \frac{\beta w_0}{2c}\right], \qquad \nu = \left[-\frac{\varepsilon_y}{\varepsilon_x}, -\frac{\varepsilon_z}{\varepsilon_y}\right] \tag{5}$$

Finally, by using the energy-balance equation, we can compute the effective axial Young's modulus as

$$E_A^* = P u_0 \big/ \varepsilon_x^2 V \tag{6}$$

where V is the RVE volume.

The effective axial shear modulus can be calculated with the same methodology described above. The boundary conditions are such that a state of pure shear is imposed. Once the constraint forces are evaluated, the shear-strain energy balance is applied:

$$\frac{1}{2}\sum \left(F_s^1 \delta_1 + F_s^2 \delta_1\right) = \frac{1}{2} G_A^* \gamma^2 A \tag{7}$$

where δ_1 is the prescribed displacement, F_s^1, and F_s^2 are the constraint forces of the shear loading cases, γ is the shear strain, and $A = 4bc$ is the RVE area.

The effective transverse Young's modulus, the effective transverse Poisson ratio, and the effective transverse shear modulus can be calculated with the same procedure.

A finite element analysis is performed at the macroscopic level; however, the composite material properties are first computed at the microscopic level. The coupling between the micro/macro approaches is attempted by a new formulation. It is assumed that the total strain is a linear combination of the elastic strain and the inelastic strain. This assumption is valid for small deformations. The fibers and the matrix are considered to be perfectly bonded. The fibers are linear elastic and the matrix is elastic–viscoplastic. From the VFD theory,[24] we have the following strain field:

$$\varepsilon_{ij}^c = c_f \varepsilon_{ij}^f + c_m \varepsilon_{ij}^m, \qquad \forall ij \neq 11 \tag{8}$$

$$\varepsilon_{ij}^c = \varepsilon_{ij}^f = \varepsilon_{ij}^m, \qquad \forall ij = 11 \tag{9}$$

where c stands for composite, f for fiber, and m for matrix, c_f is the fiber volume fraction, and c_m is the matrix volume fraction.

The decomposition of the total strain into elastic and inelastic portions leads to

$$\varepsilon_{ij}^c = c_f \left(\varepsilon_{ij}^e + \varepsilon_{ij}^p\right)_f + c_m \left(\varepsilon_{ij}^e + \varepsilon_{ij}^p\right)_m, \qquad \forall ij \neq 11 \tag{10}$$

$$\varepsilon_{ij}^c = \left(\varepsilon_{ij}^e + \varepsilon_{ij}^p\right)_f = \left(\varepsilon_{ij}^e + \varepsilon_{ij}^p\right)_m, \qquad \forall ij = 11 \tag{11}$$

With the assumption of fibers as linear and the matrix as of elastic–viscoplastic behavior, Eqs. (10) and (11) become

$$\varepsilon_{ij}^c = c_f \left(\varepsilon_{ij}^e\right)_f + c_m \left(\varepsilon_{ij}^e + \varepsilon_{ij}^p\right)_m, \qquad \forall ij \neq 11 \tag{12}$$

$$\varepsilon_{ij}^c = \left(\varepsilon_{ij}^e\right)_f = \left(\varepsilon_{ij}^e + \varepsilon_{ij}^p\right)_m, \qquad \forall ij = 11 \tag{13}$$

It is a well-known fact that the elastic strain components are related to stress by

$$\left(\varepsilon_{ij}^e\right)_c = S_{ij}^* \left(\sigma_{ij}^e\right)_c \tag{14}$$

where S_{ij}^* is the effective compliance tensor, defined for a transversely isotropic material as

$$S_{ij}^* = \begin{bmatrix} 1/E_A^* & -\nu_A^*/E_A^* & -\nu_A^*/E_A^* & 0 & 0 & 0 \\ -\nu_A^*/E_A^* & 1/E_T^* & -\nu_T^*/E_T^* & 0 & 0 & 0 \\ -\nu_A^*/E_A^* & -\nu_T^*/E_T^* & 1/E_T^* & 0 & 0 & 0 \\ 0 & 0 & 0 & 1/G_T^* & 0 & 0 \\ 0 & 0 & 0 & 0 & 1/G_A^* & 0 \\ 0 & 0 & 0 & 0 & 0 & 1/G_A^* \end{bmatrix} \tag{15}$$

Substituting Eq. (15) into Eq. (14) and the results into Eqs. (12) and (13) leads to

$$\sigma_{ij}^c = D_{ij}^* \left[\varepsilon_{ij}^c - c_m \left(\varepsilon_{ij}^p\right)_m\right] \qquad \forall ij \tag{16}$$

where $D_{ij}^* = (S_{ij}^*)^{-1}$.

A generalization of Eq. (16) is obtained when the overall composite initial strain ε_{ij}^0 and the initial stress σ_{ij}^0 are added:

$$\sigma_{ij}^c = D_{ij}^* \left[\varepsilon_{ij}^c - c_m \left(\varepsilon_{ij}^p\right)_m - \varepsilon_{ij}^0\right] + \sigma_{ij}^0 \qquad \forall ij \tag{17}$$

For a laminate, the concept of a smeared element is used. The effective elasticity tensor D_{ij}^* is substituted by the transformed elasticity tensor Q_{ij}^*:

$$Q_{ij}^* = \frac{1}{h}\int_{-h/2}^{h/2} Q_{ij}\, \mathrm{d}z \tag{18}$$

where h is the laminate thickness, z is the lamina semithickness, and Q_{ij} is the lamina transformed elasticity tensor. For more details, see Ref. 26. In this paper, thermal strains are not considered. The matrix inelastic strain rate is calculated with the model of Bodner and Partom (see Ref. 25), and it is defined as

$$\dot{\varepsilon}_{ij}^p = \frac{D_0}{\sqrt{J_2}} \exp\left[-\frac{1}{2}\left(\frac{Z^2}{3J_2}\right)^n\right] S_{ij} \tag{19}$$

where J_2 is the second deviatoric stress invariant, S_{ij} are the deviatoric stress components, Z is the Bodner hardening parameter, and D_0 and n are Bodner material constants.

The finite element approach approximates the displacement rates within an element as

$$\dot{u}_i = N_i \dot{\delta}_i \tag{20}$$

where N_i are the interpolation functions and $\dot{\delta}_i$ represent the nodal displacement rates. When the strain-displacement equations are used in the rate form, the element strain rate is given by

$$\dot{\varepsilon}_{ij} = B_{ij} \dot{\delta}_i \tag{21}$$

where B_{ij} is the strain-displacement matrix as defined by Zienkiewicz and Taylor.[27]

The usual finite element procedures are used, and for a representative element the finite element equations are obtained as

$$K_{ij} \dot{\delta}_i = \dot{F}_j^p + \dot{F}_j^\sigma + \dot{F}_j^B \tag{22}$$

where K_{ij} is the stiffness matrix, and the right-hand side is composed of the element load vectors that are due to the rate of inelastic strains, surface tractions, and body forces, respectively.

These matrices are defined by

$$K_{ij} = \int_{\Omega_e} B_{ij}^T Q_{ij}^* B_{ij} \, \mathrm{d}\Omega \tag{23}$$

$$\dot{F}_j^p = \int_{\Omega_e} B_{ij}^T D_{ij}^* \dot{\varepsilon}_{ij}^p \, \mathrm{d}\Omega \tag{24}$$

$$\dot{F}_j^\sigma = \int_{\Gamma_e} N_i^T \dot{\sigma}_{ij} \, \mathrm{d}\Gamma \tag{25}$$

$$\dot{F}_j^B = \int_{\Omega_e} N_i^T \dot{b}_i \, \mathrm{d}\Omega \tag{26}$$

The strategy used to solve the finite element equations is the following: With the initial stress distribution and internal variables predetermined, the equilibrium equations, described by Eq. (22), are used to calculate the nodal displacement rates. We then integrate the constitutive equations forward in time at the element Gauss points. With the updated values of stress and the internal variables at a new time step, the equilibrium equation is solved again. The procedure is repeated until the desired total deformation or total time is achieved.

Numerical Applications

The numerical applications presented are categorized into two groups. The first one is called the benchmark group. In this group, strain-rate tensile tests are used to validate the proposed formulations. In the second group, a practical engineering application is discussed.

SCS-6/Ti-15-3 Strain-Rate Tensile Test

The first test case is a SiC/Ti MMC, SCS-6/Ti-15-3, with a 29% fiber volume fraction. It uses a $[0_8]$ laminated rectangular specimen with nominal dimensions of $0.18 \times 1.91 \times 15.25$ cm and a constant strain rate of 0.01 1/s at 649°C. The phases are considered isotropic, and, for the fibers, E and ν are 400 GPa and 0.20, respectively. The matrix has $E = 72.5$ GPa and $\nu = 0.34$. The elastic–viscoplastic model constants given by Jeong et al.[28] are summarized in Tables 1 and 2. Note that for these test conditions the Ti-15-3 exhibits only isotropic hardening. This fact is represented by the model of Bodner and Partom when the hardening parameter m_2 is set equal to zero.

Table 1 Temperature-independent constants for Ti-15-3

D_0, 1/s	Z_1, MPa	Z_3, MPa	m_1, 1/MPa	m_2, MPa	r_1	r_2
10^4	1172.0	0.0	0.246	0.0	1.0	0.0

Table 2 Temperature-dependent constants for Ti-15-3

$Z_0 = Z_2$, MPa	A_1, 1/s	A_2, 1/s	n
621.0	0.0	0.0	3.0

Table 3 Effective elastic moduli for SCS-6/Ti-15-3

	CCA		
Property	Upper bound	Lower bound	RVE
E_A, GPa	171.7	171.1	171.4
E_T, GPa	118.1	109.7	108.0
G_A, GPa	55.2	42.5	41.0
G_T, GPa	42.6	40.3	39.8
ν_A	0.278	0.265	0.265
ν_T	0.362	0.338	0.310

Table 4 Temperature-independent constants for Ti-β21-S

D_0, 1/s	Z_1, MPa	Z_3, MPa	m_1, 1/MPa	m_2, MPa	r_1	r_2
10^4	1600.0	3700.0	0.0	10.0	3.0	3.0

Table 5 Temperature-dependent constants for Ti-β21-S

$Z_0 = Z_2$, MPa	$A_1 = A_2$, 1/s	n
1029.0	0.0887	0.82

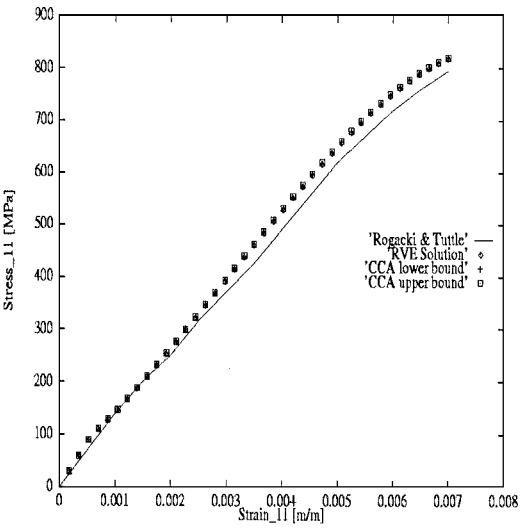

Fig. 2 Stress–strain response for SCS-6/Ti-15-3 at 649°C

The elastic moduli obtained with the CCA upper and lower bounds and the RVE approach are listed in Table 3. A slight difference (~5%) is observed on the Poisson ratio in the transverse direction. It could be due to the application of boundary conditions in the RVE finite element model. The numerical stress–strain results are compared with experimental data[29] in Fig. 2, and they seem to be in good agreement.

SCS-6/Tiβ21-S Strain-Rate Tensile Test

In this test case we wish to investigate how the model of Bodner and Partom used in this research behaves in a situation in which only kinematic hardening is present. To pursue this goal, we select a beta-phase titanium alloy (Ti-β21-S) to be the matrix of a SiC/Ti MMC with 35% fiber volume fraction. The elastic moduli for the matrix are $E = 72.0$ GPa and $\nu = 0.34$. The material constants of Bodner and Partom (from Neu[30]) are shown in Tables 4 and 5. The nonexistence of isotropic hardening is ensured by the model of Bodner and Partom when the variable m_1 is set equal to zero. The constant strain tensile test is performed at a temperature of 600°C.

Table 6 Effective elastic moduli for SCS-6/Ti-β21-S

	CCA		
Property	Upper bound	Lower bound	RVE
E_A, GPa	188.2	187.2	187.5
E_T, GPa	128.9	118.2	116.4
G_A, GPa	60.1	45.0	43.4
G_T, GPa	46.0	42.6	42.1
ν_A	0.285	0.270	0.270
ν_T	0.387	0.354	0.325

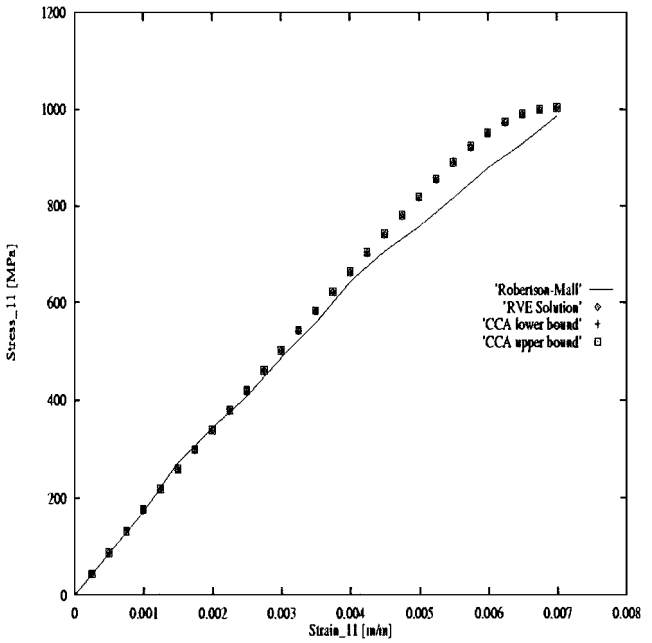

Fig. 3 Stress–strain response for SCS-6/Ti-β21-S at 600°C

The same laminated specimen dimensions and strain rate applied for the SCS-6/Ti-15-3 test case are also used here.

The effective elastic moduli obtained with the CCA and the RVE approaches are summarized in Table 6. The composite stress–strain relation is compared with experimental data from Robertson and Mall.[31] It is seen that the results obtained with the integrated micro/macro model produce a slightly stiffer response (Fig. 3). The same pattern was observed in the preceding test case. Again, the cause could be attributed to the assumption of perfect bonding and/or the homogenization process itself. However, the results presented are in reasonable agreement with those available in the literature.

Turbine Blade Tip

Mcknight et al.[32] state that the commercial air-cooled turbine blade squealer tip region has had a history of cracking. Kerrebrock[33] asserts that one of the reasons for the cracking failure of the turbine's tip is shock waves. Even though the blade inlet Mach numbers are generally small, shock losses arise from locally high Mach numbers in turbine blades. As the blade loading is increased, the velocity and the Mach number over the suction surface rise, eventually reaching supersonic values. Kerrebrock[33] also identified the fluid flow leakage at the blade tip as one of the sources of turbine efficiency decrease. Therefore cracking and damage at the turbine blade tip can be considered as major issues in the design and maintenance of turbines.

The objective here is to predict the inelastic strain field for a turbine blade tip. This information is applicable for damage prediction. Considering the present focus with three analysis possibilities, the RVE and the CCA (lower and upper bounds), the CCA upper bound was selected because it gives the highest stress values. The reason is that, with the higher values, although the turbine blade life is smaller, in a real-life maintenance procedure the conservative moduli will ensure a turbine blade change before real cracks occur, thus leading to a safer design. The analysis region is identified in

Table 7 Temperature-dependent constants for Ti-β21-S (815°C)

$Z_0 = Z_2$, MPa	$A_1 = A_2$, 1/s	n
300.0	2.0	0.55

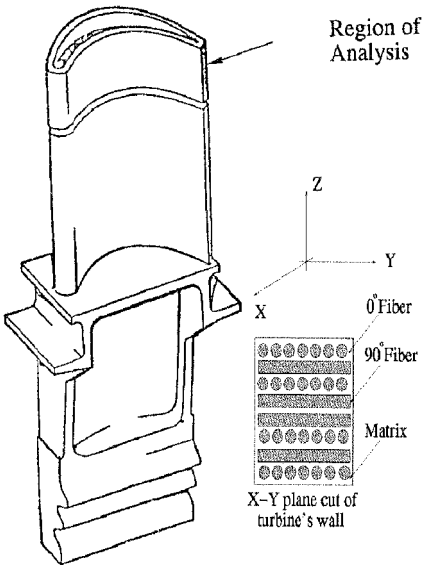

Fig. 4 Location of analysis region.

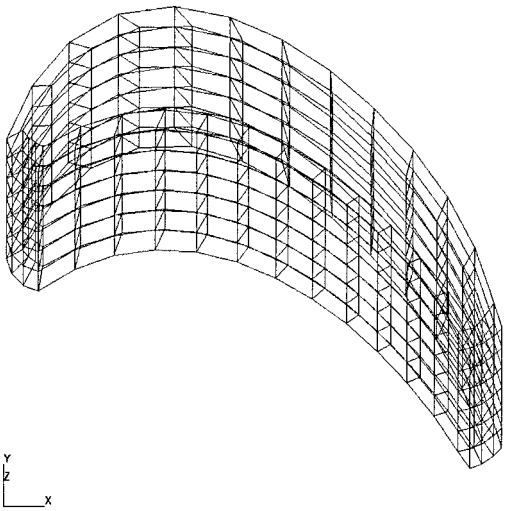

Fig. 5 Turbine blade tip: finite element mesh.

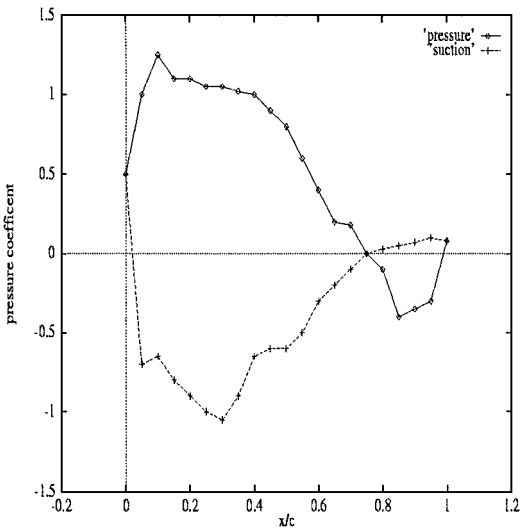

Fig. 6 Airfoil pressure distribution.

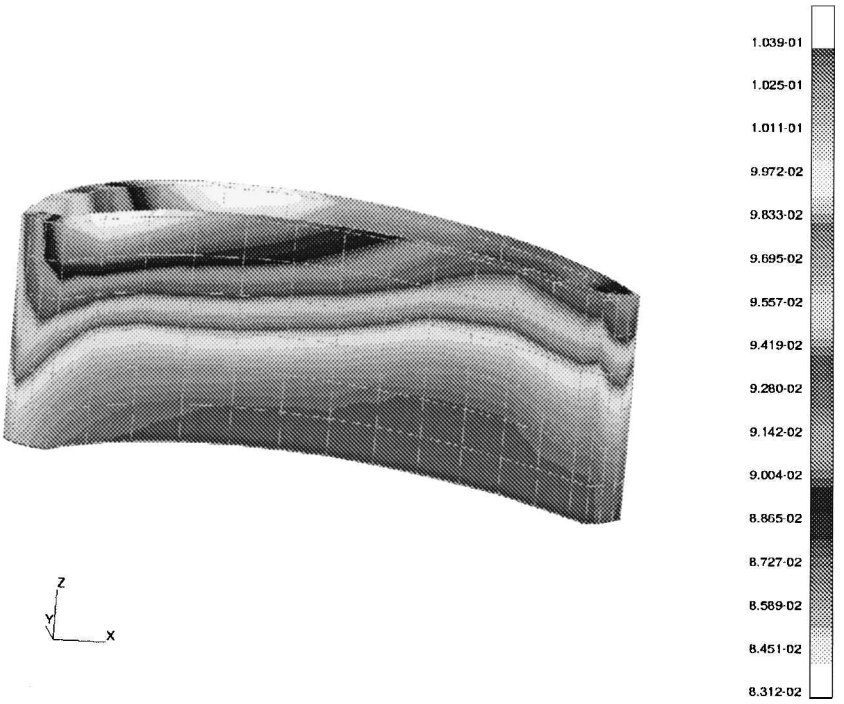

Fig. 7 Effective inelastic strain field at pressure side: Ti-β21-S.

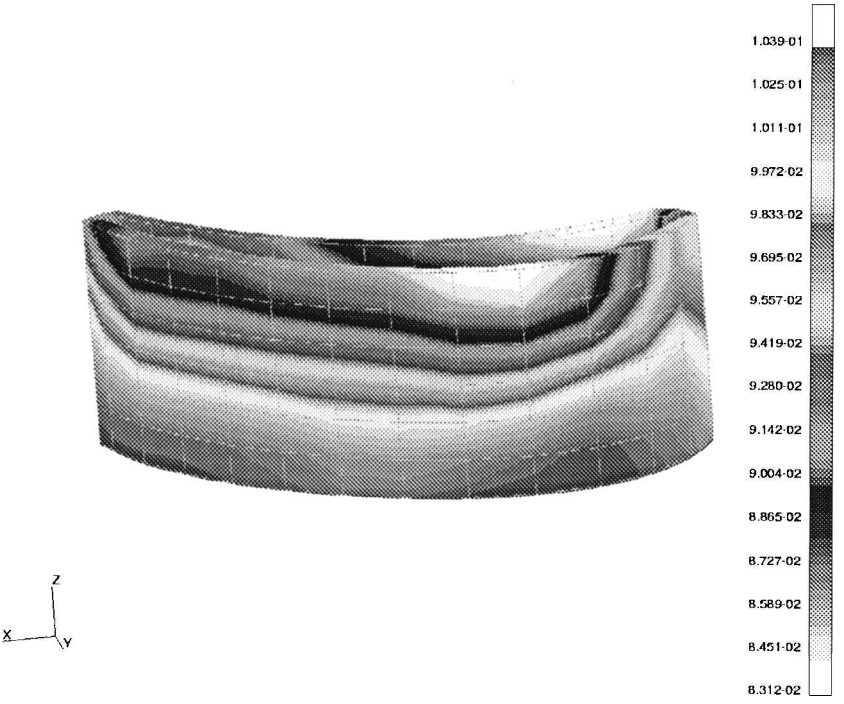

Fig. 8 Effective inelastic strain field at suction side: Ti-β21-S.

Fig. 4 and the finite element model is shown in Fig. 5. It used 180 eight-node hexahedron elements with 420 nodes and 1260 degrees of freedom.

The turbine blade's maximum span is 25.8 cm, the maximum chord is 8.71 cm, the tip span is 2.54 cm, and the blade's wall is constant and equal to 0.28 cm. These dimensions are from the paper by Chamis and Singhal,[34] who conducted a computational simulation of a real turbine blade but considered only loadings that were due to rotation. Here, both aerodynamic and centrifugal loadings are considered. The data for aerodynamic loading (pressure distribution) for a generic turbine blade at radial midsection, where a medium Reynolds number, subsonic Mach number, and steady state are assumed, are obtained from the paper by Natalini and Sciubba.[35] Figure 6 shows the fluid pressure distribution for the pressure and the suction regions. It is assumed that there is no pressure variation along the z axis. The peak pressure value used is 392 MPa, which, according to Kaufman,[36] is a realistic value. The centrifugal loading is due to the turbine blade rotation. A rotation of 1500 rpm is assumed, which is the same as that used by Chamis and Singhal.[34] The centrifugal loading forces are calculated following Mattingly et al.[37]

The turbine blade material is a SCS-6/Ti metal β21-S laminate composite $[0/90]_{2s}$ with 35% of the fiber volume fraction. It should be noted that the 0-deg direction is coincident with the z axis. The

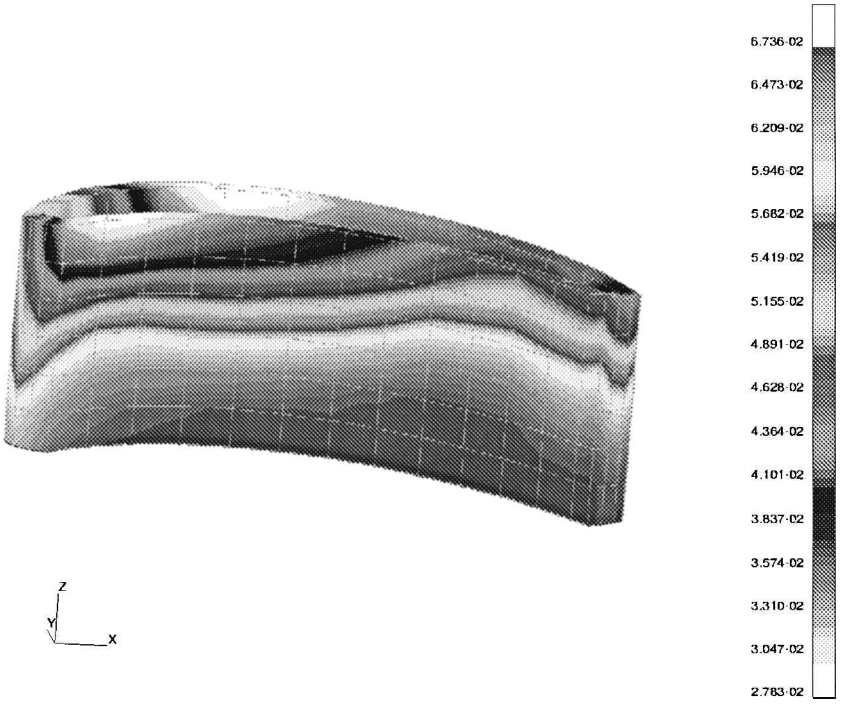

Fig. 9 Effective inelastic strain field at pressure side: MMC.

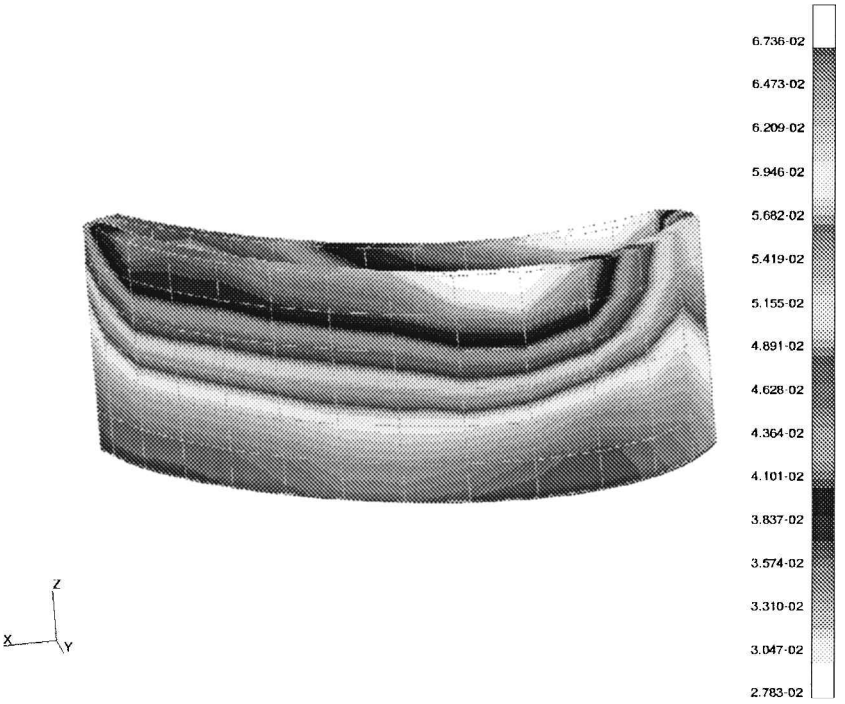

Fig. 10 Effective inelastic strain field at suction side: MMC.

temperature condition assumed is 815°C, which is an average of the temperatures used by Kaufman.[36] The matrix is assumed to follow the model of Bodner and Partom (Ref. 25), and the fibers are considered to be linear elastic. At 815°C the matrix Young's modulus is 72 GPa and the Poisson ratio value is 0.34. The SCS-6 fibers material properties are considered temperature independent and have the same material properties as those of the last two test cases. The temperature-dependent parameters of Bodner and Partom are listed in Table 7.

For comparison purposes, two numerical simulations were performed. The difference between the two simulations is restricted to the material used. In the first, the turbine blade tip is made of pure Ti-β21-S, and in the second the material used is the actual MMC described above. The first analysis is used as a benchmark parameter. The same procedure was used by Chamis and Singhal. The explicit solution algorithm, in its incremental form with the time step equal to 0.01 s, was used. The results shown in Figs. 7–10 were obtained after 50 time steps, when the inelastic strains are present. The highest effective inelastic strains occur where the nodes are constrained at the bottom. The inclusion of fiber reinforcement causes an increase in the overall material stiffness, as can be seen when the two types of analysis are compared. The same pattern of inelastic strain distribution is observed in both cases. The results are in qualitative agreement with those presented by Wilt,[38] in which a similar problem

is analyzed by use of shell elements along the midsurface of the blade, although he considers only the aerodynamic loading.

Conclusions

An integrated micro/macro mechanics procedure for structural analysis of unidirectional MMCs has been described. The model validation was performed considering the constant strain-rate tensile test for SiC/Ti MMCs (SCS-6/Ti-15-3 and SCS-6/Ti-β21-S). After the validation procedure, the integrated procedure was applied to the structural analysis of a three-dimensional finite element model of a turbine blade tip. The results indicate the following:

1) In the micromechanical analysis, in which the elastic moduli have been predicted with the RVE and the CCA approaches, the results are very encouraging.

2) In the macromechanical analysis, the present elastic–viscoplastic analysis and the integration of the micro/macro behavior closely matched with the analytical and experimental data available in the literature.

3) The three-dimensional analysis of the turbine blade tip had a qualitative agreement with other numerical results in the literature. Unfortunately, an experimental comparison of such a type of problem has not been available in the literature until now.

The integrated micro/macro procedure seems to be a promising technique for stress analysis of composite structures. The inclusion of a damage mechanism formulation is under development to bring the integrated model even closer to real applications.

Acknowledgments

The author acknowledges the financial support provided by the Brazilian Research Council and the Minas Gerais State Research Foundation. This work was presented at the American Society of Mechanical Engineers International Mechanical Engineering Congress and Exposition, November 1997, Dallas, Texas.

References

[1]Meguid, S. A., and Kalamkarov, A. L., "Asymptotic Homogenization of Elastic Composite Materials with a Regular Structure," *International Journal of Solids and Structures*, Vol. 31, No. 3, 1994, pp. 303–316.

[2]Yi, Y.-M., Park, S.-H., and Youn, S.-K., "Asymptotic Homogenization of Viscoelastic Composites with Periodic Microstructure," *International Journal of Solids and Structures*, Vol. 35, No. 17, 1998, pp. 2039–2055.

[3]Fish, J., Shek, K., Pandheeradi, M., and Shephard, M. S., "Computational Plasticity for Composite Structures Based on Mathematical Homogenization: Theory and Practice," *Computer Methods in Applied Mechanics and Engineering*, Vol. 148, No. 1, 1997, pp. 53–73.

[4]Eshelby, J. D., "The Determination of the Elastic Fields of an Ellipsoidal Inclusion and Related Problems," *Proceedings of the Royal Society of London, Series A*, Vol. 241, No. 2, 1957, pp. 376–396.

[5]Hashin, Z., and Shtrikman, S., "A Variational Approach to the Theory of the Elastic Behavior of Multiphase Materials," *Journal of the Mechanics and Physics of Solids*, Vol. 11, No. 1, 1963, pp. 127–140.

[6]Hashin, Z., and Rosen, B. W., "The Elastic Moduli for Fiber-Reinforced Materials," *Journal of Applied Mechanics*, Vol. 31, No. 2, 1964, pp. 223–232.

[7]Willis, J. R., "The Overall Elastic Response of Composite Materials," *Journal of Applied Mechanics*, Vol. 50, No. 9, 1983, pp. 1202–1209.

[8]Willis, J. R., "Variational and Related Methods for the Overall Properties of Composites," *Advances in Applied Mechanics*, Vol. 21, No. 1, 1981, pp. 1–78.

[9]Ponte Castañeda, P., and Willis, J. R., "On the Overall Properties of Nonlinearly Viscous Composites," *Proceedings of the Royal Society of London, Series A*, Vol. 416, No. 2, 1988, pp. 217–244.

[10]Christensen, R. M., *Mechanics of Composite Materials*, Wiley, New York, 1979.

[11]Talbot, D. R. S., and Willis, J. R., "Bounds of Third Order for the Overall Response of Nonlinear Composites," *Journal of the Mechanics and Physics of Solids*, Vol. 45, No. 1, 1997, pp. 87–111.

[12]Luciano, R., and Sacco, E., "Variational Methods for Homogenization of Periodic Heterogeneous Media," *European Journal of Mechanics A—Solids*, Vol. 17, No. 4, 1998, pp. 599–617.

[13]Hashin, Z., "Thermoelastic Properties of Fiber Composites with Imperfect Interface," *Mechanics of Materials*, Vol. 8, No. 4, 1991, pp. 333–348.

[14]Ponte Castañeda, P., "New Variational Principles in Plasticity and Their Application to Composite Materials," *Journal of the Mechanics and Physics of Solids*, Vol. 39, No. 1, 1992, pp. 45–71.

[15]Aboudi, J., "Micromechanical Analysis of Composites by the Methods of Cells," *Applied Mechanical Review*, Vol. 49, No. 7, 1989, pp. S83–S91.

[16]Sun, C. T., and Vaidya, R. S., "Prediction of Composite Properties from a Representative Volume Element," *Composite Science and Technology*, Vol. 56, No. 2, 1996, pp. 171–179.

[17]Drugan, W. J., and Willis, J. R., "A Micromechanics-Based Nonlocal Constitutive Equation and Estimates of Representative Volume Element Size for Elastic Composites," *Journal of the Mechanics and Physics of Solids*, Vol. 44, No. 4, 1996, pp. 497–524.

[18]Chun, H.-J., and Daniel, I. M., "Behavior of Unidirectional Metal Matrix Composites Under Thermomechanical Loading," *Journal of Engineering Materials and Technology*, Vol. 118, No. 3, 1996, pp. 310–316.

[19]Mori, T., and Tanaka, K., "Average Stress in Matrix and Average Elastic Energy of Materials with Misfitting Inclusions," *Acta Metallurgica*, Vol. 21, No. 5, 1973, pp. 571–574.

[20]Kodiyalam, S., Parthasarathy, V. N., Hartle, M. S., and McKnight, R. L., "Ply Layup Optimization and Micromechanics Tailoring of Composite Aircraft Engine Structures," *Journal of Propulsion and Power*, Vol. 10, No. 8, 1994, pp. 897–905.

[21]Aboudi, J., Pindera, M.-J., and Arnold, S. M., "New Coupled Micro-Macro Continuum Theory for Functionally Graded Materials," *Proceedings of 10th Conference on Engineering Mechanics*, Vol. 2, American Society of Mechanical Engineers, New York, 1995, pp. 1191–1194.

[22]Tamma, K. K., and Ávila, A. F., "An Integrated Micro/Macro Modeling and Computational Methodology for High Temperature Composites," *Thermal Stress V*, edited by R. B. Hetnarski, Lastran Corp., Honeoeye Falls, NY, 1999, pp. 143–256.

[23]Hashin, Z., "Analysis of Properties of Fiber Composite with Anisotropic Constituents," *Journal of Applied Mechanics*, Vol. 46, No. 6, 1979, pp. 543–550.

[24]Dvorak, G. J., and Bahei-El-Din, Y. A., "Plasticity Analysis of Fibrous Composites," *Journal of Applied Mechanics*, Vol. 49, No. 3, 1982, pp. 327–335.

[25]Bodner, S. R., "Review of Unified Elastic–Viscoplastic Theory," *Unified Constitutive Equations for Plastic Deformation and Creep of Engineering Alloys*, edited by A. Miller, Elsevier Science, New York, 1987, pp. 77–106.

[26]Ávila, A. F., "An Integrated Methodology and Formulations for Micro/Macro Modeling and Analysis of Metal Matrix Composites," Ph.D. Dissertation, Dept. of Mechanical Engineering, Univ. of Minnesota, 1996, pp. 96–135.

[27]Zienkiewicz, O. C., and Taylor, R. L., *The Finite Element Method*, McGraw–Hill, New York, 1989, pp. 206–259.

[28]Jeong, G. S., Allen, D. H., and Lagoudas, D. C., "Residual Stress Evolution Due to Cool Down in Viscoplastic Metal Matrix Composites," *Thermomechanical Behavior of Advanced Structures Materials*, edited by D. Coker, American Society of Mechanical Engineers, New York, 1993, pp. 17–31.

[29]Rogacki, J. R., and Tuttle, M., "An Investigation of the Thermoviscoplastic Behavior of a Metal Matrix Composite at Elevated Temperatures," NASA CR-190700, 1992.

[30]Neu, R. W., "Nonisothermal Material Parameters for Bodner and Partom Model," *Material Parameter Estimation for Modern Constitutive Equations*, edited by R. Kroupa, American Society of Mechanical Engineers, New York, 1993, pp. 211–226.

[31]Robertson, D. D., and Mall, S., "Micromechanical Analysis for Thermoviscoplastic Behavior of Unidirectional Fibrous Composites," *Composite Science and Technology*, Vol. 50, No. 5, 1994, pp. 483–496.

[32]Mcknight, R. L., Laflen, J. H., and Spamer, G. T., "Turbine Blade Tip Durability Analysis," NASA CR-165268, 1981.

[33]Kerrebrock, J. L., *Aircraft Engines and Gas Turbine*, MIT Press, Cambridge, MA, 1992.

[34]Chamis, C. C., and Singhal, S. N., "Coupled Multi-Disciplinary Simulation of Composite Engine Structures in Propulsion Environment," NASA TM-105575, 1992.

[35]Natalini, G., and Sciubba, E., "Entropy Generation Rates in Air-Cooled Turbine Nozzles," *Proceedings of the 8th Congress and Exposition on Gas Turbines in Cogeneration and Utility, Industrial and Independent Power Generation*, American Society of Mechanical Engineers, New York, 1994, pp. 723–743.

[36]Kaufman, A., "Elastic-Plastic Structural Analysis for Cooled Turbine Blades Airfoils," NASA TP-1679, 1980.

[37]Mattingly, J. D., Heiser, W. H., and Daley, D. H., *Aircraft Engine Design*, AIAA, New York, 1987, pp. 222–324.

[38]Wilt, T. E., "Linear and Nonlinear Finite Element Analysis of Laminated Composite Structures at High Temperatures," Ph.D. Dissertation, Dept. of Mechanical Engineering, Univ. of Akron, Akron, OH, 1992.

S. Saigal
Associate Editor